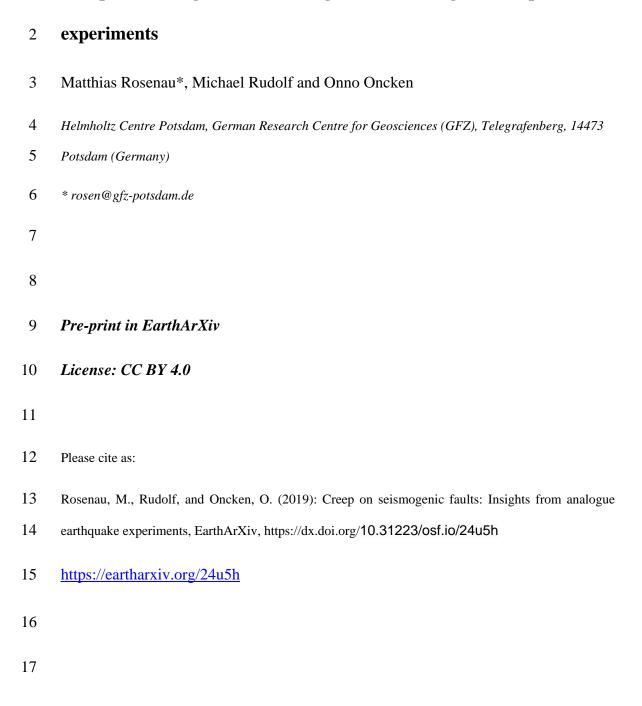
Rosenau et al_creep_on_seismogenic_faults v.4

03.06.2019

1 Creep on seismogenic faults: Insights from analogue earthquake



18 **Highlights**

- Stick-slip experiments mimic seismogenic fault behavior
- Creep and earthquakes are not mutually exclusive fault styles
- Interseismic creep varies systematically with fault properties and stress state

22

23

24 Keywords

25 friction, faults, granular materials, aseismic creep, earthquakes, precursors

Abstract

27

28 Tectonic faults display a range of slip behaviors including continuous and episodic 29 slip covering rates of more than 10 orders of magnitude (<mm/a to >m/s). The 30 physical control of such kinematic observations remains ambiguous. To gain insight 31 into the slip behavior of brittle faults we performed laboratory stick-slip experiments 32 using a rock analogue, granular material. We realized conditions under which our 33 seismogenic fault analogue shows a variety of slip behaviors ranging from slow, 34 quasi continuous creep to episodic slow slip to dynamic rupture controlled by a 35 limited number of parameters. We explore a wide parameter space by varying loading 36 rate from those corresponding to interseismic to postseismic rates and normal loads 37 equivalent to hydrostatic to lithostatic conditions at seismogenic depth. The 38 experiments demonstrate that significant interseismic creep and earthquakes may not 39 be mutually exclusive phenomena and that creep signals vary systematically with the 40 fault's seismic potential. Accordingly, the transience of interseismic creep scales with 41 fault strength and seismic coupling as well as with the maturity of the seismic cycle. 42 Loading rate independence of creep signals suggests that mechanical properties of 43 faults (e.g. seismic coupling) can be inferred from shortterm observations (e.g. 44 aftershock sequences). Moreover, we observe the number and size of small episodic 45 slip events to systematically increase towards the end of the seismic cycle providing 46 an observable proxy of the relative shear stress state on seismogenic faults. Modelling 47 the data suggest that for very weak faults in a late stage of their seismic cycle, the 48 observed creep systematics may lead to the chimera of a perennially creeping fault 49 releasing stress by continuous creep and/or transient slow slip instead of large 50 earthquakes.

1. Introduction

Faults in the brittle part of the lithosphere may slip at rates ranging from slow,
aseismic (< 1 mm/a) to fast, seismic (> 1m/s) (Peng and Gomberg, 2010, and
references therein). Moreover they might do so in either continuous (i.e. at constant
rate) or transient fashion (at changing rate). Modern geodetic methods allow
monitoring fault slip rates over time scales long enough to cover a significant part of
the loading history (generally decades) for some fast loading settings like plate
boundaries thereby constraining their kinematic behavior with unprecedented
resolution (Moreno et al., 2010; Shirzaei and Bürgmann, 2013). Accordingly, a suite
of slip behaviors has been observed ranging from continuous creep (e.g., Bokelman
and Kovach, 2003) to transient creep (e.g. precursory and afterslip) (e.g. Bedford et
al., 2013, Schurr et al., 2014) to episodic slip events at various rates (earthquakes,
slow slip and non-volcanic tremor, low frequency earthquakes, creep events) (e.g.
Rogers and Dragert, 2003; Ide et al., 2007). High fluid pressure has been identified as
a controlling factor for slow slip phenomena (e.g., Peng and Gomberg, 2010, Moreno
et al, 2014) but the underlying mechanisms and mechanics controlling which slip
behavior prevails remain under determined. Importantly the physics of such faulting is
often intrinsically undeterminable in nature because of the inaccessibility of the
source and the ambiguity of the geophysical and kinematic observation which can be
fitted by more than one theoretical models and/or set of model parameters.
Seismic and aseismic slip behavior are conventually viewed as mutually exclusive at a
given location through time. Typically "ambivalent" fault slip behaviors are modelled
as a result of the interaction of spatially separated sources, e.g. a seismogenic patch
(asperity) embedded in an aseismic area (barriers) (e.g., Wei et al., 2013). However, a
more integrative view of slow and fast slip phenomena might be possible where the

slip behavior is non-unique (e.g. Peng and Gomberg, 2010). Indeed, there is recent evidence from longterm geodetic observations as well as contrasting geodeticseismological versus palaeoseismological observations that given fault areas might be more variable in their slip behaviors than conventionally believed. In particular we now have to acknowledge that a particular fault area may show aseismic creep or slow slip at one time while failing catastrophically in dynamic earthquake ruptures at others. Examples of spatially overlapping seismic and aseismic fault areas have been found along the Hayward fault in California U.S. (Lienkaemper at al., 2012, Shirzaei and Bürgmann, 2013) as well along the subduction megathrusts off Japan (Loveless and Meade, 2011, Kato et al, 2012) and Chile (Moreno et al, 2010, Ruiz et al, 2014). As a reaction to such evidence for non-unique slip behavior, existing friction laws have been adapted for example by allowing aseismic creep at low slip rates but dynamic weakening at high slip rates, e.g. in the presence of fluids (e.g. Noda and Lapusta, 2013). We here contribute to the discussion of creep signals by means of experimental modeling seismogenic fault slip behavior using a labscale fault analogue under conditions relevant to natural faulting. We show that few parameters can control the rate and stability of fault slip and demonstrate that creeping faults can generate earthquakes. Showing the systematics by which this happens allows inferring information on the mechanical properties and state of the fault from kinematic observations.

2. Friction regimes

77

78

79

80

81

82

83

84

85

86

87

88

89

90

91

92

93

94

95

96

97

98

101

99 The most established view on the mechanics of faulting in the brittle regime (< c. 100 350°C) is represented by the rate-and-state dependent friction law (e.g. Scholz, 1998). This law opens avenues to explain fault slip behavior over a range of rates. In

particular, it relates aseismic and seismic fault behavior to an intrinsic velocity-strengthening and velocity-weakening fault property, respectively. Accordingly, once static friction is overcome a velocity-weakening fault may weaken dynamically as slip accelerates resulting in a runaway effect or instability and nucleating an earthquake. In contrast, an increase of dynamic friction along a velocity strengthening fault inhibits earthquake nucleation at all times. Importantly, a third regime exists, in which most of the natural faults might actually be, which is characterized by velocity weakening under sufficiently low effective normal stress σ_n ' (e.g. near the surface or at high pore fluid pressures). In this regime, which is called the conditionally stable regime, fault slip is slow and stable under quasi-static loading while it can become unstable under dynamic loading (acceleration). "Sufficiently" low effective normal stress in the context of conditional stability means that the externally applied normal load minus the local pore fluid pressure is below a critical value σ_0 :

115
$$\sigma_{\rm n}' < \sigma_{\rm c} = kL / -(a-b)$$
 (i)

where k is the spring stiffness in the original theoretical spring slider framework (or the stiffness of the medium in which the fault is embedded), a the instantaneous change of friction following a loading rate change (so-called direct velocity effect) and b the new steady state friction (so-called evolutionary effect) after the loading rate change which evolves over the characteristic slip distance L (a physical interpretation is the size of asperities). The combined parameter a-b is negative for velocity weakening interfaces and positive for velocity-strengthening interfaces. Its absolute values are typically measured in the lab to be in the order of few percent for rocks and other materials (Scholz, 1998; and references therein).

3. Analogue earthquake experimental setup

The laboratory-scale analogue earthquake experiments presented here have been
performed in a ring shear tester setup (RST, Figure 1) where a granular material (dry
rice) is sheared rotary in a velocity stepping test under imposed normal loads while
shear stress is measured continuously (e.g. Rosenau et al., 2017, Rudolf et al., 2019).
The rate of laboratory fault slip has been inferred from displacement records derived
by particle image velocimetry (PIV, LaVision Strainmaster ®). For PIV analysis, a 12
bit monochrome charged-coupled device (CCD) camera shot sequential images of the
analogue fault through a transparent shear cell at a frequency of 10 Hz. The particle
motions between successive images are then determined by cross-correlation of
textural differences (i.e., gray values) formed by groups of particles within
interrogation windows using a Fast Fourier Transform algorithm (Adam et al. 2003).
Precision and accuracy of the PIV method is better than 0.1 px of the original image
which scales to the order of micrometer in the presented setup.
The stiffness of the loading system (\sim 1.3 kN/mm) together with a - b (\sim -0.015) and L
(~ 2 μ m) for dry rice (Rosenau et al., 2009) predicts a critical (effective) normal stress
of $\sigma_c = 8$ kPa. Accordingly, we performed the tests at $1-16$ kPa normal load to
explore the slip behavior of natural faults across the bifurcation. We refer to the high
(8, 16 kPa) and low (1, 2, 4 kPa) normal stress experiments as strong and weak faults,
respectively.
Similarity of the experimental simulation with its natural prototype is ensured by
keeping the following dimensionless numbers the same: (1) the friction coefficient
(ratio between yield strength and normal stress) $\mu \sim 0.7$, (Byerlee, 1978) and (2) a
friction rate parameter a-b ~ -0.015 similar to rocks (e.g., Scholz, 1998) as well as (3)

a dimensionless stress drop (ratio between rupture slip and length) of $\Delta \tau^* \sim 10^{-5} - 10^{-4}$ similar to earthquakes (e.g., Scholz, 1989). Applying a stress scale of 1:10.000, the setup generates slip instabilities (aka "analogue earthquakes", Figure 2) with stress drops which scale to 1 - 100 MPa in nature typical of large intra- and interplate earthquakes (Scholz, 1989; Hardebeck and Aron, 2009) including precursory events of different scale (Figure 3). The strength of the laboratory fault analogues can be interpreted in two way: Either representing (A) different crustal depths at a given pore fluid pressure (i.e. weak = shallow, strong = deep) or (B) representing different pore fluid pressures at a given depth. For example, at typical seismogenic crustal depths of 5 – 15 km and typical rock densities of 2300 – 2700 kg/m³, the experimental normal stresses (10 – 160 MPa) would correspond to pore fluid pressures of 38 – 96 % lithostatic pressure, i.e. from hydrostatic to near lithostatic. Time is not explicitly scaled in the experiments but imposed loading rates cover more than two orders of magnitude (0.1 - 25 mm/min) similar to post- and interseismic deformation rates in nature (mm/day – mm/year) in order to test possible time scale dependencies (or independencies) of creep signals.

4. Experimental observations and analysis

150

151

152

153

154

155

156

157

158

159

160

161

162

163

164

165

166

167

168

169

170

171

172

173

174

Analogue fault slip in our experiments is characterized by quasi-periodic stress drops (Figure 2). Quasi-periodic stress drops are preceded by smaller, episodic events (Figure 3). The sizes and recurrence intervals of periodic stress drops are systematically related to the applied normal load and loading rate (Figure 4). This observation is consistent with normal load and loading rate both determining the yield strength according to rate-and-state friction theory (Scholz, 1998). A regular stick-slip behavior is consistent with a characteristic earthquake model where episodic slip occurs at a certain stress level determined by the yield strength and causes relaxation

175 to a certain lower stress level determined by the residual friction and the stiffness of 176 the loading system. 177 Beside periodic and episodic stress drops, representing slip during earthquakes and 178 slow slip events, a significant amount of long-term laboratory fault slip occurs as 179 transient creep (accelerating stable slip) between episodic failures. This stable slip 180 during the "stick"-phase causes the stress curves in Figures 2 and 3 to deviate from a 181 linear, elastic loading path. Instead of an ideal "saw tooth" pattern characterizing 182 stress histories of perfect stick-slip, a "shark fin" pattern emerges for the observed 183 stick-creep-slip. In the experiments, up to 80 % of long-term fault slip might be taken 184 up by creep at low effective normal stresses resulting in seismic coupling coefficients 185 (the ratio of seismic to total fault slip) of <0.2 for very weak faults (Figure 2C). At 186 high normal stresses, seismic coupling increases to >0.8 for strong faults in the 187 experiments. 188 Detailed inspection of the stress loading paths (Figure 5 A) and interseismic creep 189 signals (Figure 5 B) and their time-derivates (i.e. loading and slip rates, Figure 5 C 190 and D) sheds light on the time and stress dependencies of laboratory fault creep. 191 Accordingly, stress in the inter-event time (which is normalized to a unit interval 192 here) accumulates in a more transient, non-linear fashion for weak faults than it does 193 for strong faults (red versus blue curves in Figure 5 A and C). Strong faults show a 194 stressing rate which is almost consistent with elastic loading except prior to an event 195 (i.e. runs parallel long-term rate in Figure 5 C) while stressing rates of weak faults 196 vary by more than an order of magnitude. Slip varies consistently with loading. 197 Accordingly, slip accumulates in a more non-linear for strong faults than it does for 198 weak faults (Figure 5 B) covering two orders of magnitude in slip rate versus less than 199 one, respectively (Figure 5 D).

Connecting stress and strain allow us to describe the creep behavior of our fault analogues as follows: Creep along strong laboratory faults accelerates at rather constant stressing rate late in the interseismic period leading to episodic failure ("precursory slip"). Weak faults instead creep at higher rates throughout the interseismic period but more continuously and at progressively decreasing stressing rate. Moreover, strong faults reach only about half of the long-term fault slip rate towards the very end of the loading cycle, whereas weak faults may creep at almost the long-term rate for the second half of the loading cycle. In order to analyze the creep behavior systematically as controlled by extrinsic factors (normal stress and loading rate) we attempted to quantify the non-linearity (or transience) of stress and slip accumulation by a single, dimensionless parameter. Therefore we calculated the area beneath the normalized stress and strain accumulation curves in Figure 5 A and B, respectively, which we call the unit stress and unit strain integrals (Figure 5E). Clearly, these measures of transience decrease systematically with increasing applied normal stress or fault strength as expected from the observations before. However, they do not correlate with loading rate, an observation that is not intuitive but useful as will be discussed below. The positive correlation between the unit stress and slip integrals (Figure 5F) indicates the consistency of our independent stress and stain observations and is a direct result of the intrinsic velocity weakening behavior of the laboratory fault. Irrespective of fault strength, episodic slip events of various speeds occur at high stress level modulating the interseismic creep signal in the late stage of the analogue seismic cycle (Figure 3). Preliminary analysis suggests that these precursor events increase systematically in number and size as the fault evolves towards failure.

224

200

201

202

203

204

205

206

207

208

209

210

211

212

213

214

215

216

217

218

219

220

221

222

5. Discussion

5.1 Inversion of fault properties and state from creep signals

The observation of continuous and transient creep signals as well as episodic slow slips which are systematically linked to fault properties and maturity of the loading cycle or stress level but independent of loading rate bear important implications for the interpretation of fault creep records as observable proxies for fault strength and seismic potential. Fault creep records in nature are generally short with respect to the seismic cycle. The results obtained here suggest that any creep record, though only a snapshot of the full seismic cycle, might bear important information on long-term fault properties and hazardous behavior.

Using the analog fault observations from the here presented experiments, an empirical inversion scheme as proposed in Figure 6 can be applied, where inaccessible fault properties like fault strength, seismic coupling, stress drop and recurrence interval can be inferred from the observable transience of interseismic creep signals. Here, creep transience (CT) is defined as

240
$$CT = 2 \cdot (1 - 2 \cdot \text{unit slip integral})$$
 (ii)

in order to derive a dimensionless (and therefore scale-independent) parameter which varies between 0 (linear strain accumulation) and 1 (non-linear, highly transient strain accumulation).

Linear regression analysis of the experimentally derived data plotted in such a scheme indicates a significant correlation between creep signals and fault properties and behavior but independence of loading rate. More specifically, fault strength, seismic coupling, stress drop as well as recurrence period show a positive linear or log-linear dependency with CT ($R^2 > 0.6 - 0.8$).

Importantly, no significant correlations exist between any of the parameters with loading rate. This is indicated by the rather horizontal or scattered distribution of data from subsets with the same fault strength measured at different velocities in Figure 6 as well as the collapse of time-series data from such subsets in Figure 5. The fact that the systematics found experimentally are loading rate independent suggest that shortterm observations can be extrapolated to larger earthquakes and longer recurrence intervals. I.e. this timescale independency opens the opportunity to generalize fault properties or behavior derived during aftershocks sequences or earthquake swarms or from repeating events to longterm (multiple seismic cycles) fault behavior. An observation not quantified in detail here is the occurrence of precursor slip events of different scale and velocity which systematically increase in number and size towards the end of a seismic cycle (Figure 3). Several large earthquakes in subduction zones have actually been preceded by accelerating foreshock activity (e.g. Bouchon et al., 2013). Especially the recent 2014 8.1 Pisagua earthquake offshore Chile showed accelerating foreshock activity with a decrease in b-value (representing an increase in the number of large events relative to small events) over the decade preceding the main shock (Schurr et al., 2014). If such a systematic behavior can be generalized and physically explained it should lead to a better ability to forecast earthquakes.

249

250

251

252

253

254

255

256

257

258

259

260

261

262

263

264

265

266

267

268

269

270

271

272

273

5.2 Revisiting creep records along the San Andreas Fault

In order to test and apply our proposed inversion scheme, we use the longest creep records available and revisit the San Andreas Fault data. California creepmeters have been installed across the San Andreas Fault in the late 1960s (Schulz et al., 1982), geodetic surveys took place since the mid-1970s (Burford and Harsh, 1980; Lisowski and Prescott, 1981) and surface velocities from space-geodetic measurements are available since about a decade (e.g., Bürgmann et al., 2000; Titus et al., 2006). For a

274	mean recurrence interval of large Californian earthquakes of about 150 ± 50 years
275	along any SAF segment (e.g. Zielke et al., 2010), the observation time frame
276	generally represents less than half of the seismic cycle length. Nevertheless, the
277	records are probably the best data we can get today.
278	Seismic and aseismic strike-slip along the central SAF (cSAF) accounts for most of
279	the Pacific-Great Valley microplate relative motion in central California (Thatcher,
280	1979; Lisowski and Prescot, 1981, Titus et al., 2006; Rolandone et al., 2008; Ryder
281	and Bürgmann, 2008). As suggested by over 40 years of creep and earthquake
282	records, the central section of the cSAF creeps continuously at a decadal scale at
283	about 28 mm/a at seismogenic depth (0 – 12 km, Schulz et al., 1982, Titus et al.,
284	2006, Rolandone et al., 2008). This long-term creep is modulated by shorter term
285	transients presumably very shallow (< 5 km) and related to earthquakes (Lisowski and
286	Prescott, 1981; Thurber, 1996). At seismogenic depths repeating microearthquakes
287	occur (Nadeau and McEvilly, 2004) indicating that locally and/or transiently, velocity
288	weakening behavior is established along the fault. Noticeably, the current creep of
289	cSAF is only about $80 - 90$ % of the far-field, tectonic loading rate $(31 - 35 \text{ mm/a},$
290	Titus et al., 2006, Rolandone et al., 2008; Ryder and Bürgmann, 2008) suggesting a
291	slip deficit of few millimeter accumulating each year. Right-lateral shear strains in the
292	sidewalls of the cSAF are evidently very small (Rolandone et al., 2008, Savage, 2009)
293	suggesting a small stressing rate. Episodic slow slip events as they occur late in the
294	interseismic period in our experiments (Figure 3) have been reported as potential
295	earthquake pre-cursors along the SAF by Thurber (1996) and Thurber and Sessions
296	(1998) based on temporal cross-correlation of creepmeter records and seismological
297	catalogues. Though the correlations they found were statistically significant, the
298	feedback mechanism remained unclear. Noticeably, they did not find a clear spatial

299	relation between the loci of creep and earthquakes which would be required by our
300	model. Moreover, they assigned creep to the very shallow crust (<5 km) and not to
301	seimogenic depths. Whilst the adjoining segments ruptured in large earthquakes in
302	1906 (San Francisco) and 1857 (Fort Tejon), the creeping section of the cSAF has not
303	experienced large earthquakes in the historic past (~300 years).
304	In the light of the experiments done in this study the key question is: Does the absence
305	of large earthquakes, the high and continuous creep rates as well as the low shear
306	strain accumulation serves as a good indicator that this fault segment poses no seismic
307	hazard?
308	Applying the empirical inversion scheme established above (Figure 6), we would
309	infer first that the creeping section of the cSAF is a very weak fault based on the
310	rather linear slip accumulation signal (Schulz et al., 1982, Titus et al., 2006) and low
311	stressing rate (Rolandone et al., 2008, Savage, 2009). This is consistent with previous
312	findings based on the observation of low resolved shear stresses along the creeping
313	section and absence of a heat flow anomaly (Brune et al., 1969, Lachenbruch and
314	Sass, 1980, Zoback et al., 1987).
315	The cSAF shows therefore kinematic similarity to our weak fault analogue
316	characterized dynamically by low seismic coupling and small stress drops during
317	earthquakes. This may however not mean that the seismic potential is low. In contrast:
318	Because stress drop is only a weak measure of earthquake size, which scales
319	dominantly with the rupture area, and because low seismic coupling (or vice versa a
320	large amount of interseismic creep) just stretches the recurrence intervals of
321	potentially large earthquakes. We will elaborate on this effect in the next section.

5.3 Modelling the effect of creep on recurrence time and the chimera of

323 perennially creeping faults

Because of the empirically found correlation between fault strength and creep, the net effect of creep on the recurrence interval of earthquakes should not only take into account the stretching of the recurrence interval due to creep but also a modification of recurrence interval due to changes in strengths (Figure 4). Such a scenario is illustrated in Figure 7.

Quantitatively, creep lengthens the (effective) recurrence interval to

330
$$t^* = 1/(1\text{-creep}).$$
 (iii)

For example a fault where 50 % of longterm slip is accommodated aseismically requires twice as much time to reach a certain stress level again. However, because creep correlates with fault weakness and weaker faults fail at lower stress level in quicker succession for the same far field stressing rate (Figure 4), this lengthening effect is to some degree counterbalanced by shorter recurrence intervals.

In Figure 7 we plot the effective recurrence time observed in our experiments in relation to creep on faults of variable strength and model the data as the combined result of the competing effects of "creep lengthening" (according to eq. (iii)) and "weakness shortening". The latter effect is taken into account by fitting an exponential relation of the form

$$t^{**}=e^{-A} \times creep$$
 (iv)

to the data. Parameter A is an empirically derived proxy for the relation between strength and recurrence interval and varies between 4 and 6 in our example. The net effect of "creep lengthening" and "weakness shortening" of recurrence intervals, i.e. the effective recurrence interval, is then simply

 $t = t^* x t^{**} = 1/(1-\text{creep}) e^{-(-A x \text{ creep})}.$ (v)

For the parameter space realized in our experiments recurrence time is always shorter than on faults without creep, i.e. the weakness effect dominates the recurrence behavior such that more creeping faults have systematically shorter recurrence times. However, at least theoretically our model predicts for very weak faults (not realized in our experiments) with very low seismic coupling coefficients and very high creep amounts, the lengthening effect should start dominating and consequently the effective recurrence intervals should become longer than without creep. For creep amounts exceeding 98% effective recurrence times may well exceed any historical record for fast creeping faults (Figure 7). In the extreme such a seismically nearly uncoupled, very weak fault appears as seismically silent over many human generations – obviously a chimera.

5.4 Creep on continental vs. subduction megathrusts

Locking pattern of continental and subduction megathrusts show a striking qualitative difference: While continental megathrusts, e.g. the Himalayan main thrust, show homogeneous and high locking with little interseismic creep (Stevens and Avouac, 2015), subduction megathusts, like the Chilean subduction zone, show a patchy locking pattern indicating a significant amount of creep (e.g. Saillard et al., 2017). According to our experiments, and in line with theory, such a qualitative difference can be explained by higher amounts water entrained into subduction megathrust compared to continental settings, lowering the effective normal load and this enhancing creep. However, other explanations exist like differences in lithology and even lack of offshore geodetic coverage.

6 Conclusion

Based on stick-slip experiments using a labscale fault analogue, we explored the slip behavior of seismogenic faults and tested the potential to derive information on fault properties and state from kinematic observables. We showed that the stress buildup between episodic failures (analogue earthquakes) is non-linear and anti-correlated with the creep signals. According to our experiments the transience of stress buildup and creep is controlled primarily by fault normal stress, i.e. related to frictional strength and/or pore-fluid pressure, and systematically reflect the seismic coupling coefficient and maturity of the seismic cycle. Application of these systematics to the creeping section of the central San Andreas fault suggests that this fault branch may not be aseismic on the long term (millennia scale) but is in a late stage of a seismic cycle which exceeds historic records. The qualitative difference in creep on megathrusts between homogenously fully locked continental versus heterogeneously locked subduction megathrusts may be similarly explained by the presence of water in oceanic settings.

Acknowledgements

This study has been partially funded by the German Research Foundation (DFG) collaborative research center SFB1114 "Scaling Cascades in Complex Systems", project B01.

390	Figure Captions
391	Figure 1: Analogue earthquake experimental setup: (A) side (camera) view of the
392	sample (rice) in a transparent shear cell in situ in the ring-shear tester, boundary
393	conditions and observables indicated; PIV velocities are representative of a slip event.
394	(B) sketch of the ring-shear tester setup (modified from Schulze (2003)) with PIV
395	camera position indicated.
396	Figure 2: Stress and strain time-series of laboratory faults: (A) Stress time series
397	measured during velocity stepping tests under variable normal loads simulating
398	seismic and aseismic slip along very weak to strong fault slip. Note the periodic stress
399	drops representing analogue earthquakes. (B) Slip time series for very weak and
400	strong faults derived by PIV. (C) Variation of seismic coupling over the parameter
401	space tested here. Note the sensitivity of seismic coupling to normal load and
402	insensitivity to loading rate.
403	Figure 3: Examples of precursory slip events along laboratory faults (from Rosenau
404	et al., 2017): (A) stress time series, (B) Histogram of number of slow slip events per
405	unit interseismic time interval. Note the increase of precursory events in size and
406	number towards the end of the seismic cycle.
407	Figure 4: Dependency of recurrence interval and stress drop on loading rate and
408	normal load over the parameters space tested here.
409	Figure 5: Systematics of interseismic stress-strain relationships for laboratory faults:
410	(A) interseismic stress accumulation (normalized), (B) interseismic slip accumulation

(normalized), (C) interseismic stress rate (normalized), (D) interseismic slip rate

(normalized), (E) Variation of unit stress and slip integrals over the parameter space

411

413 tested here, (F) correlation of unit stress and slip integrals indicating velocity 414 weakening behaviour. 415 **Figure 6:** Dependency of creep signal transience on laboratory fault properties: (A) 416 fault strength as a function of creep transience, (B) seismic coupling as a function of 417 creep transience, (C) stress drop as a function of creep transience, (D) recurrence 418 period as a function of creep transience. 419 **Figure 7:** Modelling the effect of fault creep and strength on recurrence time of 420 earthquakes. Experimental data are fitted by theoretical model taking into account two 421 competing effect: Fault creep lengthens recurrence intervals ("creep lengthening 422 effect") while weakening faults should shorten recurrence intervals ("weakness 423 shortening effect"). The effective recurrence is dominated by the weakness effect for 424 faults creeping up to 98%. However, faults which accumulate >98 % of fault slip 425 aseismically may still generate earthquakes with recurrence periods exceeding 426 historical records (California earthquake history shown as example). 427

428 **References:**

- 1. Adam, J., O. Oncken, N. Kukowski, J. Lohrmann, S. Hoth, J. L. Urai, W. van
- der Zee, J. Schmatz, B. Wieneke, and K. Pfeiffer (2005), Shear localisation
- and strain distribution during tectonic faulting New insights from granular-
- flow experiments and high-resolution optical image correlation
- techniques, Journal of Structural Geology, 27(2), 183-301.
- 2. Bedford, J., et al. (2013), A high-resolution, time-variable afterslip model for
- the 2010 Maule Mw=8.8, Chile megathrust earthquake, Earth and Planetary
- 436 Science Letters, 383, 26-36.
- 3. Bokelmann, G. H. R. (2003), Long-term creep-rate changes and their
- causes, Geophysical Research Letters, 30(8).
- 4. Bouchon, M., V. Durand, D. Marsan, H. Karabulut, and J. Schmittbuhl (2013),
- The long precursory phase of most large interplate earthquakes, Nature
- 441 Geoscience, 6(4), 299-302.
- 5. Brune, J. N., T. L. Henyey, and R. F. Roy (1969), Heat flow, stress, and rate of
- slip along the San Andreas Fault, California, Journal of Geophysical
- 444 Research, 74(15), 3821--3827.
- 6. Burford, R. O., and P. W. Harsh (1980), Slip on the San Andreas fault in
- central California from alinement array surveys, Bulletin of the Seismological
- 447 Society of America, 70(4), 1233-1261.
- 448 7. Byerlee, J. (1978), Friction of rocks, Pageoph, 116, 615-626.
- 8. Bürgmann, R., D. Schmidt, R. M. Nadeau, M. d'Alessio, E. Fielding, D.
- 450 Manaker, T. V. McEvilly, and M. H. Murray (2000), Earthquake Potential

- Along the Northern Hayward Fault, California, Science, 289(5482), 1178-
- 452 1182.
- 9. Hardebeck, J. L., and A. Aron (2009), Earthquake Stress Drops and Inferred
- 454 Fault Strength on the Hayward Fault, East San Francisco Bay,
- 455 California, Bulletin of the Seismological Society of America, 99(3), 1801-
- 456 1814.
- 10. Ide, S., G. C. Beroza, D. R. Shelly, and T. Uchide (2007), A scaling law for
- 458 slow earthquakes, Nature, 447(7140), 76-79.
- 459 11. Kato, A., K. Obara, T. Igarashi, H. Tsuruoka, S. Nakagawa, and N. Hirata
- 460 (2012), Propagation of Slow Slip Leading Up to the 2011 M-w 9.0 Tohoku-
- 461 Oki Earthquake, Science, 335(6069), 705-708.
- 12. Lachenbruch, A. H., and J. H. Sass (1980), Heat flow and energetics of the
- San Andreas Fault Zone, Journal of Geophysical Research: Solid
- 464 Earth, 85(B11), 6185--6222.
- 13. Lienkaemper, J. J., J. N. Baldwin, R. Turner, R. R. Sickler, and J. Brown
- 466 (2013), A Record of Large Earthquakes during the Past Two Millennia on the
- Southern Green Valley Fault, California, Bulletin of the Seismological Society
- 468 of America, 103(4), 2386-2403.
- 14. Lisowski, M., and W. H. Prescott (1981), Short-range distance measurements
- along the San Andreas fault system in central California, 1975 to
- 471 1979, Bulletin of the Seismological Society of America, 71(5), 1607-1624.
- 472 15. Loveless, J. P., and B. J. Meade (2011), Spatial correlation of interseismic
- coupling and coseismic rupture extent of the 2011 MW= 9.0 Tohoku-oki
- earthquake, Geophysical Research Letters, 38(17).

- 16. Moreno, M., M. Rosenau, and O. Oncken (2010), 2010 Maule earthquake slip correlates with pre-seismic locking of Andean subduction
- zone, Nature, 467(7312), 198-202.
- 478 17. Moreno, M., C. Haberland, O. Oncken, A. Rietbrock, S. Angiboust, and O.
- Heidbach (2014), Locking of the Chile subduction zone controlled by fluid
- pressure before the 2010 earthquake, Nature Geoscience, 7(4), 292-296.
- 18. Nadeau, R. M., and T. V. McEvilly (2004), Periodic Pulsing of Characteristic
- 482 Microearthquakes on the San Andreas Fault, Science, 303(5655), 220-222.
- 483 19. Noda, H., and N. Lapusta (2013), Stable creeping fault segments can become
- destructive as a result of dynamic weakening, Nature, 493(7433), 518-+.
- 20. Peng, Z. G., and J. Gomberg (2010), An integrated perspective of the
- continuum between earthquakes and slow-slip phenomena, Nature
- 487 Geoscience, 3(9), 599-607.
- 488 21. Rogers, G., and H. Dragert (2003), Episodic tremor and slip on the Cascadia
- subduction zone: The chatter of silent slip, Science, 300, 1942-1943.
- 490 22. Rolandone, F., R. Bürgmann, D. C. Agnew, I. A. Johanson, D. C. Templeton,
- 491 M. A. d'Alessio, S. J. Titus, C. DeMets, and B. Tikoff (2008), Aseismic slip
- and fault-normal strain along the central creeping section of the San Andreas
- fault, Geophysical Research Letters, 35(14), n/a--n/a.
- 494 23. Rosenau, M., J. Lohrmann, and O. Oncken (2009), Shocks in a box: An
- analogue model of subduction earthquake cycles with application to
- seismotectonic forearc evolution, Journal of Geophysical Research, 114(B1).

- 497 24. Rosenau, M., F. Corbi, S. Dominguez (2017): Analogue earthquakes and
- seismic cycles: Experimental modelling across timescales, Solid Earth, doi:
- 499 10.5194/se-2016-165
- 500 25. Rudolf, M., Rosenau, M., Ziegenhagen T., et al. (2019): Smart speed imaging
- in Digital Image Correlation: Application to seismotectonic scale modelling,
- Front. Earth Sci., https://doi.org/10.3389/feart.2018.00248
- 503 26. Ruiz, S., M. Metois, A. Fuenzalida, J. Ruiz, F. Leyton, R. Grandin, C. Vigny,
- R. Madariaga, and J. Campos (2014), Intense foreshocks and a slow slip event
- preceded the 2014 Iquique Mw 8.1 earthquake, Science.
- 506 27. Ryder, I., and R. Bürgmann (2008), Spatial variations in slip deficit on the
- central San Andreas Fault from InSAR, Geophysical Journal
- 508 International, 175(3), 837--852.
- 509 28. Saillard, M., L. Audin, B. Rousset, J. P. Avouac, M. Chlieh, S. R. Hall, L.
- Husson, and D. L. Farber (2017), From the seismic cycle to long-term
- deformation: linking seismic coupling and Quaternary coastal geomorphology
- along the Andean megathrust, *Tectonics*, 36(2), 241-256.
- 513 29. Savage, J. C. (2009), Comment on "Aseismic slip and fault-normal strain
- along creeping section of the San Andreas Fault" by F. Rolandone et
- al., Geophysical Research Letters, 36(13), n/a--n/a.
- 30. Scholz, C. H. (1989), Mechanics of Faulting, Ann. Rev. Earth Planet. Sci., 17,
- 517 309-334.
- 31. Scholz, C. H. (1998), Earthquakes and friction laws, Nature, 391, 37-42.

519 32. Schulze, D. (2003), Time- and velocity-dependent properties of powders 520 effecting slip-stick oscillations, Chemical Engineering & Technology, 26(10), 521 1047-1051. 522 33. Schurr, B., et al. (2014), Gradual unlocking of plate boundary controlled 523 initiation of the 2014 Iquique earthquake, Nature, 512(7514), 299-+. 524 34. Shirzaei, M., and R. Buergmann (2013), Time-dependent model of creep on 525 the Hayward fault from joint inversion of 18 years of InSAR and surface creep 526 data, Journal of Geophysical Research-Solid Earth, 118(4), 1733-1746. 527 35. Stevens, V.L., Avouac, J.-P. (2015), Interseismic coupling on the main 528 Himalayan thrust. Geophysical Research Letters, doi:10.1002/2015GL064845 529 36. Thatcher, W. (1979), Horizontal crustal deformation from historic geodetic 530 measurements in southern California, Journal of Geophysical Research: Solid 531 Earth, 84(B5), 2351--2370. 532 37. Thurber, C. H. (1996), Creep events preceding small to moderate earthquakes 533 on the San Andreas fault, Nature, 380, 425 - 428. 534 38. Titus, S. J., C. DeMets, and B. Tikoff (2006), Thirty-Five-Year Creep Rates 535 for the Creeping Segment of the San Andreas Fault and the Effects of the 2004 536 Parkfield Earthquake: Constraints from Alignment Arrays, Continuous Global Positioning System, and Creepmeters, Bulletin of the Seismological Society of 537 America, 96(4B), S250-S268. 538 539 39. Wei, M., Y. Kaneko, Y. J. Liu, and J. J. McGuire (2013), Episodic fault creep 540 events in California controlled by shallow frictional heterogeneity, Nature 541 Geoscience, 6(7), 566-570.

40. Zielke, O., J. R. Arrowsmith, L. G. Ludwig, and S. O. Akçiz (2010), Slip in
the 1857 and Earlier Large Earthquakes Along the Carrizo Plain, San Andreas
Fault, Science, 327(5969), 1119-1122.
41. Zoback, M. D., et al. (1987), New Evidence on the State of Stress of the San
Andreas Fault System, Science, 238(4830), 1105-1111.